Journal of Advanced Ceramics
2013, 2(2): 119–127
DOI: 10.1007/s40145-013-0049-x ISSN 2226-4108

Research Article

Dielectric behavior of $CaCu_3Ti_4O_{12}$ electro-ceramic doped with La, Mn and Ni synthesized by modified citrate-gel route

Laxman SINGH[a], U. S. RAI[a], Alok Kumar RAI[b], K. D. MANDAL[c,*]

[a]*Department of Chemistry*, *Centre of Advanced Study*, *Faculty of Science*, *Banaras Hindu University*, *Varanasi 221005*, *U.P.*, *India*
[b]*Department of Materials Science and Engineering*, *Chonnam National University*, *300 Yongbong-dong*, *Bukgu*, *Gwangju 500-757*, *Republic of Korea*
[c]*Department of Applied Chemistry*, *Indian Institute of Technology*, *Banaras Hindu University*, *Varanasi 221005*, *U.P.*, *India*

Received: December 12, 2012; Revised: January 29, 2013; Accepted: February 20, 2013

Abstract: The effect of La^{3+}, Mn^{2+} and Ni^{2+} doped calcium copper titanate, $CaCu_3Ti_4O_{12}$ (CCTO), at higher concentrations (CR1 and CR2 with 5 mol% and 10 mol%, respectively), has been examined by semi-wet route at relatively lower temperature. This semi-wet route employs citrate–nitrate gel chemical method using TiO_2 solid powders. X-ray diffraction (XRD) analysis confirms the formation of single phase in the doped samples sintered at 900 ℃ for 8 h. Scanning electron micrographs (SEM) show that the average grain size for CR2 is larger than that of CR1 composition. The energy dispersive X-ray spectroscopy (EDX) is used to study the percentage compositions of different ions present in both ceramics. Dielectric constant (ε_r) and dielectric loss ($\tan\delta$) values of CR1 are comparatively higher than those of CR2 ceramic at all measured frequencies and temperatures. The nature of temperature-dependent relaxation behavior of the ceramics is also studied by impedance, modulus spectroscopic analysis and confirms Maxwell–Wagner relaxation.

Keywords: oxide materials; chemical synthesis; dielectric properties; grain boundaries; X-ray diffraction (XRD)

1 Introduction

Recently, much attention has been paid to an unusual cubic perovskite oxide material $CaCu_3Ti_4O_{12}$ (CCTO), due to its high dielectric constant (10^4–10^5) and good stability over a wide temperature range from 100 K to 600 K [1–4]. The large dielectric constant is very unusual because it does not show ferroelectric behavior. Giant dielectric constant of CCTO has been attributed to Maxwell–Wagner effect [5] at the interface of grains and grain boundaries in earlier studies, while Lunkenheimer *et al*. [6] believed that it is due to the electrode polarization effect. The materials with high ε_r can store more charge and the smaller electronic circuits can be designed. It is considered as a very potential material for applications in microelectronics, especially in capacitive components and varistors. Partial substitution of appropriate cations in CCTO is considered as an effective method to improve the physical properties of the materials. The radius, valancy and co-ordination number of an element are important parameters to determine the site it occupies

* Corresponding author.
E-mail: kdmandal.apc@itbhu.ac.in

in the parent compound and the composition range of solid solution formation [7]. It is well known that the dielectric properties of CCTO are strongly dependent upon the processing condition as well as doping effects [8,9]. A lot of research work has been done on partial substitution of Cu and Ti ions in CCTO ceramic in order to improve the dielectric properties for understanding the origin of dielectric response in these materials [10,11]. In the previous work, various substitutions were made on different sites of CCTO to investigate the effect of substitution on dielectric properties, e.g., Ca by La [12], Cu by Mn [13] and Ti by Ni [14]. In the present communication, La^{3+}, Mn^{2+} and Ni^{2+} cations doped calcium copper titanate, CCTO, at higher concentration level (5 mol% and 10 mol%), were synthesized by semi-wet route at relatively lower temperature and abbreviated as CR1 and CR2 for 5 mol% and 10 mol%, respectively. The surface morphology, dielectric properties, relaxation behavior of the doped ceramics have been examined.

2 Experimental procedures

Analytical reagent grade chemicals $Ca(NO_3)_2{\cdot}4H_2O$, $La(NO_3)_3{\cdot}6H_2O$, $Cu(NO_3)_2{\cdot}3H_2O$, $Ni(NO_3)_2{\cdot}6H_2O$, $Mn(CH_3COO)_2{\cdot}4H_2O$, titanium dioxide ($TiO_2$) and citric acid, all having purity of 99.95% obtained from Merck, India, were used as starting materials. Standard solutions of metal nitrates were prepared using distilled water. Solutions of metal nitrates in stoichiometric amount of these metal ions were mixed in a beaker. Calculated amount of TiO_2 and citric acid equivalent to metal ions were added to the solution. The solution was heated on a hot plate using a magnetic stirrer at 70–90 ℃ to evaporate water and dried at 100–120 ℃ in hot air oven for 12 h to yield a blue gel. The gel was calcined in air at 800 ℃ for 6 h in a muffle furnace. The resultant mixtures were ground into fine powders using a pestle and a mortar. Cylindrical pellets were made using a hydraulic press. The pellets were sintered at 900 ℃ for 8 h in air. In order to perform the electrical measurements, silver paste was applied to both sides of the circular face of the ceramic pellets, then dried at 600 ℃ for 20 min, and cooled naturally to room temperature. The crystalline phases of the sintered samples were identified using an X-ray diffractometer (Rich-Siefert, ID-3000) employing Cu Kα radiation. The microstructures of the fractured surfaces were examined using a scanning electron microscope (SEM, JEOL JSM5410). The energy dispersive X-ray analyzer (EDX, Kevex, Sigma KS3) was used for elemental analysis of the sintered samples. The dielectric and impedance data of the doped CCTO ceramics were collected using the LCR (inductance, capacitance and resistance) meter (PSM 1735, Newton 4th Ltd, U.K.) with variation in frequency (100 Hz–5 MHz) and temperature (300–500 K).

3 Results and discussion

The X-ray diffraction (XRD) patterns of CR1 and CR2 ceramics sintered at 900 ℃ for 8 h are shown in Fig. 1. The doped CCTO precursor dry powders were calcined at 800 ℃ for 6 h and then sintered at 900 ℃ for 8 h. XRD data were indexed on the basis of cubic unit cell similar to the undoped CCTO. The similarity of the doped X-ray data to the undoped CCTO (JCPDS 75-2188), confirms the formation of a single-phase material. There is no evidence of the presence of a secondary phase in the ceramic. The lattice parameter and unit cell volume were determined using the least-square refinement method. The value of lattice parameter and its unit cell volume for both compositions are given in Table 1. The lattice parameter increases with the dopant concentration

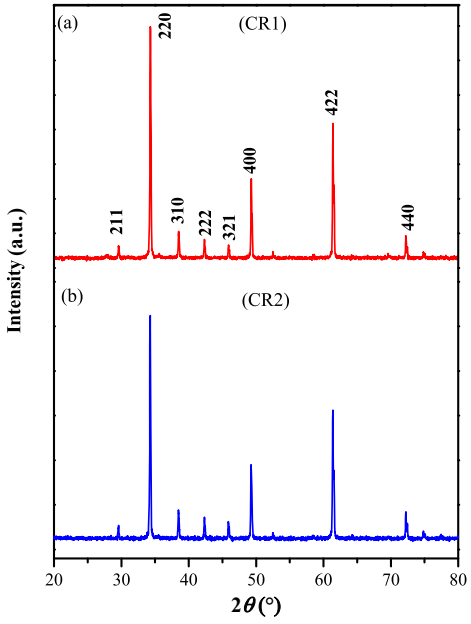

Fig. 1 XRD patterns of (a) CR1 and (b) CR2 sintered at 900 ℃ for 8 h.

Table 1 Crystal system, lattice parameter and unit cell volume for CR1 and CR2 ceramics

System	Composition x	Crystal system	Lattice parameter a (Å)	Unit cell volume a^3 (Å^3)
$Ca_{1-x}La_xCu_{3-x}Mn_xTi_{4-x}Ni_xO_{12}$	0.05	Cubic	7.3877	403.2051
	0.10	Cubic	7.6591	449.2992

increasing. The slight increase in lattice parameter and unit cell volume is due to the small difference in ionic radii of the substituent ions and the host ions [15].

To investigate the role of microstructure and composition on the dielectric properties of these ceramics, SEM and EDX studies were performed for both materials. Figure 2 shows the SEM images of the fractured surface of both compositions sintered at 900 ℃ for 8 h. The SEM image for CR1 shows faceted-packed morphology having grain size in the range of 1–2 μm. The SEM image for CR2 shows faceted grains with cubical appearance morphology. It is clearly seen that the microstructure of the doped CCTO ceramic changes significantly with the value of x increasing. The grain size for CR2 composition is found to be in the range of 1–3 μm and there is an indication of agglomeration of a secondary phase along the grain boundaries. This is due to the transition of copper oxide into the liquid phase during sintering treatment [16,17]. This suggests that the specimens prepared in the present study have a polycrystalline structure. From Figs. 2(a) and 2(b), it seems that the grain size increases remarkably on the increasing of the dopant concentration x. The modification of grain size affects the dielectric response in CCTO as reported earlier, but it should not be greater than 20 μm [18]. The grain size of these ceramics synthesized by this method is relatively smaller than those synthesized by the conventional ceramic methods [19,20].

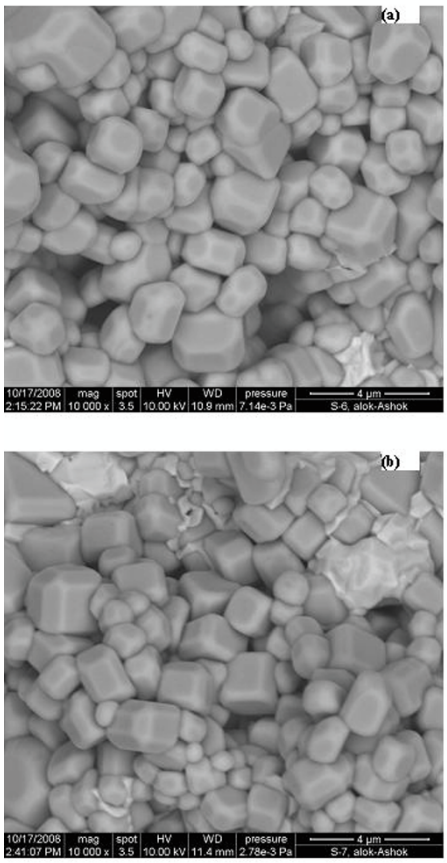

Fig. 2 SEM micrographs of (a) CR1 and (b) CR2 sintered at 900 ℃ for 8 h.

The EDX spectra obtained for CR1 and CR2 (Fig. 3), clearly show the presence of Ca^{2+}, La^{3+}, Cu^{2+}, Mn^{2+}, Ti^{4+} and Ni^{2+} in both ceramics. The atomic percentages of the major ions, i.e., Ca^{2+}, Cu^{2+}, Ti^{4+} and O^{2-} present in CR1 ceramic are 7.37%, 27.75%, 36.32% and 28.51%, respectively, whereas in CR2 their respective compositions are 7.25%, 26.05%, 34.27% and 29.92%. In both compositions, the major ions are present as per stoichiometric ratio and confirm the purity of CR1 and CR2 ceramics prepared by the semi-wet route.

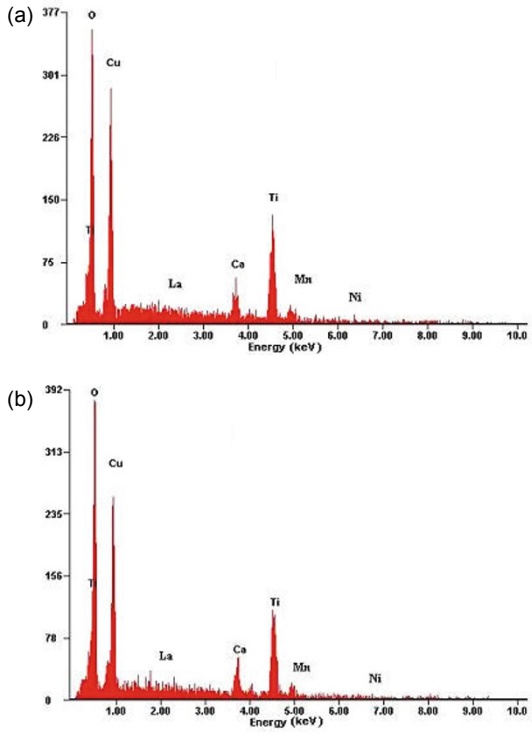

Fig. 3 EDX spectra of (a) CR1 and (b) CR2 sintered at 900 ℃ for 8 h.

The temperature dependence of dielectric constant (ε_r) and dielectric loss (tanδ) of the doped CCTO samples under different frequencies between 100 Hz and 100 kHz are shown in Figs. 4 and 5. It is noted from Fig. 4 that the dielectric constant of CR1 is ~1164 at room temperature (310 K) and 100 Hz, which increases continuously with temperature increasing and becomes more rapid beyond 425 K. Dielectric constant of CR2 is ~510 at room temperature and 100 Hz, and also increases with temperature increasing as shown in Fig. 5.

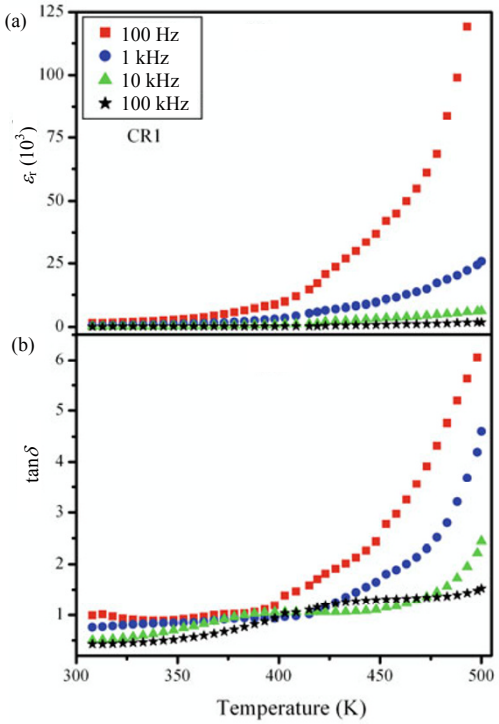

Fig. 4 The variation of dielectric constant (ε_r) and dielectric loss (tanδ) with temperature at a few selected frequencies for CR1 ceramic.

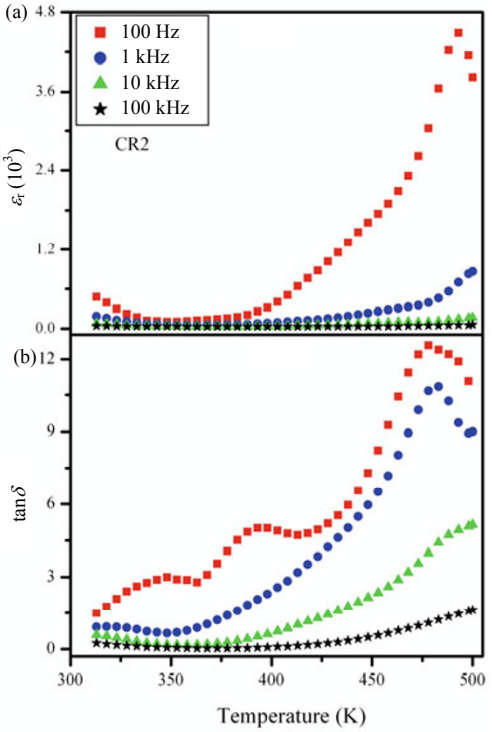

Fig. 5 The variation of dielectric constant (ε_r) and dielectric loss (tanδ) with temperature at a few selected frequencies for CR2 ceramic.

It is found that dielectric constant (ε_r) at low frequency is quite higher than that at high frequency. The result is similar to that of dielectric properties of CCTO as a function of temperature in the lower-frequency region [21]. The dielectric constants of CR1 and CR2 ceramics at 10 kHz and 100 kHz are almost independent in the temperature range of 300–425 K, and then increase steadily. It is also observed that the dielectric constants of CR1 are always higher than those of CR2 ceramic for all measured frequencies. This is due to the larger grain size of CR2 than CR1. It is noted that the tanδ values of CR1 and CR2 ceramics at room temperature and 100 kHz are 0.46 and 0.02, respectively. The tanδ values for CR2 remain constant in the temperature range of 310–425 K, and then increase steadily with the rise in temperature at high frequency (100 kHz). The plots of tanδ at low frequency show anomaly at 480 K.

The plots of variation of dielectric constant (ε_r) and dielectric loss (tanδ) of these samples with frequency at a few selected temperatures are shown in Figs. 6 and 7. As seen from the figures, dielectric constants of both ceramics decrease with the increase in frequency.

The dielectric constant of CR1 is always higher than that of CR2 ceramic in the measured frequency range of 100 Hz–5 MHz. The rate of decrease of ε_r with frequency increases with temperature increasing. It is observed from Fig. 6 that the dielectric loss also decreases with frequency increasing. As we increase the temperature, the dielectric loss also increases in low-frequency regions. It is observed from Fig. 7 that the broadening of the peaks shows typical relaxation behavior found in CR2 ceramic at low frequency with temperature increasing. These peaks shift to lower-frequency region with temperature decreasing [22]. This relaxation behavior arises due to space charge polarization present in these ceramics. The

grain boundary barrier layer capacitor consists of conducting or semi-conducting grains and insulating grain boundary layers. Therefore, relaxation behavior arises whenever two phases with different electrical conductivities are in contact.

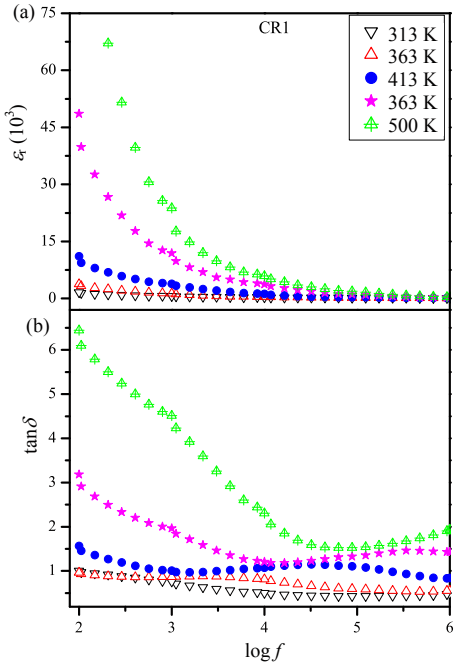

Fig. 6 The variation of dielectric constant (ε_r) and dielectric loss (tanδ) vs. log f for CR1 ceramic at a few selected temperatures.

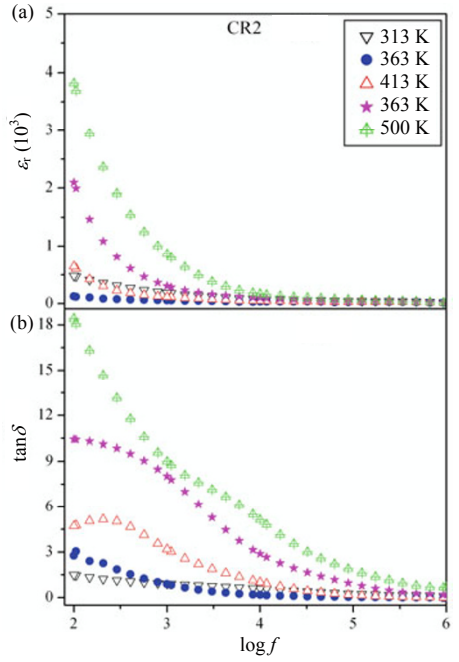

Fig. 7 The variation of dielectric constant (ε_r) and dielectric loss (tanδ) vs. log$f$ for CR2 ceramic at a few selected temperatures.

The investigation of dielectric relaxation and formation of barrier layer in this ceramic is confirmed by complex plane impedance (Z^*) and complex plane modulus (M^*) analysis, which separates the contributions of grains, grain boundaries and electrode specimen interface to the total resistance and capacitance, respectively, and correlates the electrical behavior of the ceramic to its microstructure [23]. This structure can be modeled using an equivalent impedance circuit that consists of two parallel resistance–capacitance (RC) elements in series. One pair of the parallel RC elements represents the grain boundary layers, while the other pair of parallel RC elements represents the grains. The capacitance C_{gb} and resistance R_{gb} of the grain boundary layers are usually much larger than the capacitance C_g and resistance R_g of the grains. Therefore, the relaxation time $\tau_{gb}=R_{gb}C_{gb}$ of the grain boundary layers is much larger than that of the grains $\tau_g=R_gC_g$. In this case, two parallel RC elements in series produce two semicircular arcs in a complex impedance plane Z^* plot [24] and the impedance can be calculated from the following equations:

$$Z^* = \frac{1}{R_g^{-1}+\mathrm{i}\omega C_g}+\frac{1}{R_{gb}^{-1}+\mathrm{i}\omega C_{gb}} = Z'-\mathrm{i}Z'' \quad (1)$$

where

$$Z' = \frac{R_g}{1+(\omega R_g C_g)^2}+\frac{R_{gb}}{1+(\omega R_{gb}C_{gb})^2} \quad (2)$$

and

$$Z'' = R_g\left[\frac{\omega R_g C_g}{1+(\omega R_g C_g)^2}\right]+R_{gb}\left[\frac{\omega R_{gb}C_{gb}}{1+(\omega R_{gb}C_{gb})^2}\right] \quad (3)$$

Z' is the real part of the complex impedance and Z'' is the imaginary part. The large arc is due to the grain boundary responses at the low frequencies, and the small arc is due to the grain responses at the high frequencies. At the maximum of an arc $\omega\tau=2\pi f_{max}\tau=1$, where $\omega=2\pi f$, f is the frequency of the applied field. In actual measurements, it is difficult to obtain both semicircular arcs in one Z^* plot, especially for the small arc associated with the grains. Its f_{max} at room temperature is well beyond the highest available frequency of impedance analyzers used. Figure 8 shows the complex impedance plane Z^* plots of CR1 and CR2 ceramics obtained at temperatures 313 K and 413 K, respectively. The grain boundary response of CR1 dominates at 313 K as shown in the inset of Fig. 8(a). The grain boundary resistivity of CR1 and CR2 are 122.44×10^5 Ω·cm and 151.48×10^5 Ω·cm,

respectively, at room temperature (313 K). The resistivity of grain boundary (R_{gb}) for CR1 and CR2 are 3.25×10^5 Ω·cm and 12.36×10^5 Ω·cm at 413 K, respectively. It is observed from Fig. 8(b) and its inset that the grain resistivity of CR2 are 70.64×10^5 Ω·cm and 10.68×10^5 Ω·cm at 313 K and 413 K, respectively. It is observed that on increasing the dopants concentration, the resistivity of CR2 is higher than that of CR1 at both temperatures. In the case of CR1, the existence of single arc can be taken to interpret both the grain and grain boundary conduction processes have identical time constant at both temperatures, while CR2 shows the semi-circle arcs at both temperatures but overlapped. The overlapped semicircle arcs between grain and grain boundary may be due to the molten grain and the formation of undefined grain boundaries [25].

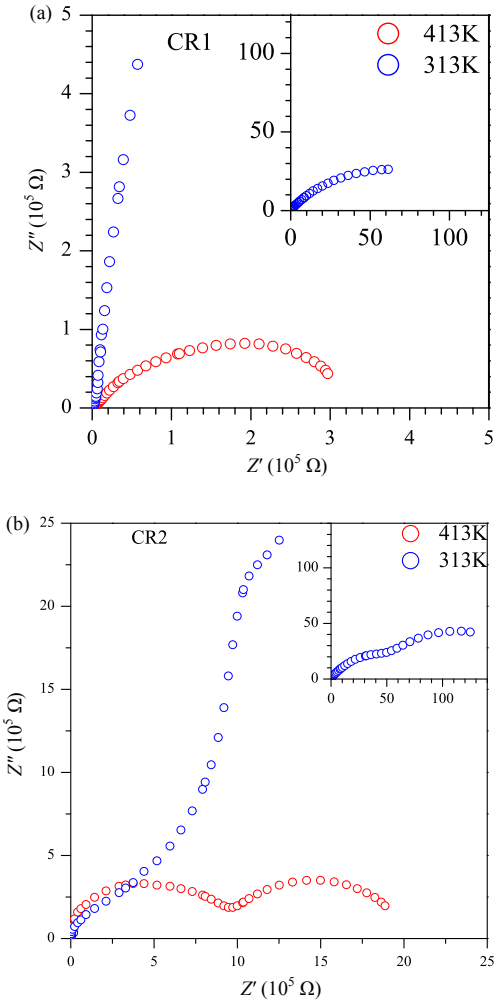

Fig. 8 Complex impedance plane plots vs. measuring temperature for (a) CR1 and (b) CR2 ceramics. The inset in (a) and (b) show the expended view of CR1 and CR2 at 313K, respectively.

The variation of the imaginary part of the impedance Z'' with frequency at a few selected temperatures is shown in Figs. 9 and 10 for CR1 and CR2, respectively. The inset figures are the expanded view of Figs. 9 and 10 at high temperature. It clearly shows that the relaxation peaks are observed at all measured temperatures for both ceramics. In the case of CR2 ceramic, they show relaxation peaks at low frequency and high frequency. The peaks are suppressed and slightly shifted to high-frequency region on increasing temperature, which confirms the existence of a temperature-dependent dielectric relaxation. The dispersion of curves in the low-frequency region at different temperatures is very clear and appears to be

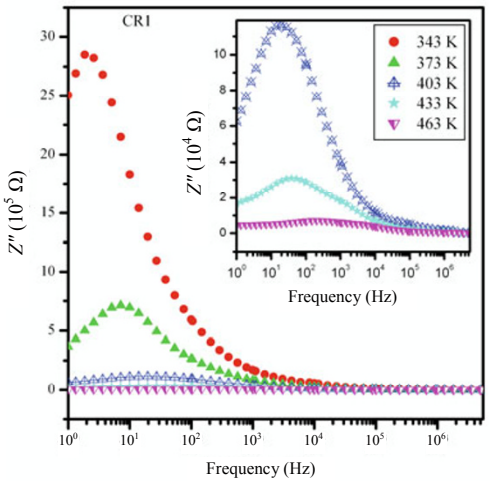

Fig. 9 Impedance plane plots Z'' vs. frequency at a few selected temperatures for CR1 sintered at 900 ℃ for 8 h. The inset shows an expended view at high temperature.

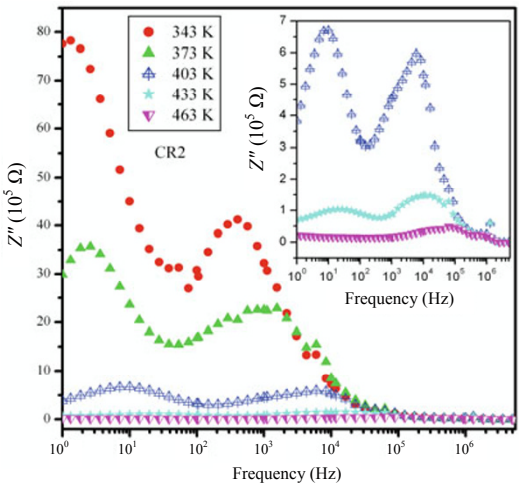

Fig. 10 Impedance plane plots Z'' vs. frequency at a few selected temperatures for CR2 sintered at 900 ℃ for 8 h. The inset shows an expended view at high temperature.

merging at higher frequency with temperature. This behavior is apparently due to the presence of space charge polarization effect at lower frequency which is definitely eliminated at higher frequency.

In order to investigate the temperature dependence of relaxation processes in these ceramics, the electric modulus studies were also carried out. The complex electric modulus (M^*) is defined in terms of the complex dielectric constant (ε^*) and is represented as

$$M^* = (\varepsilon^*)^{-1} \tag{4}$$

$$M' + \mathrm{i}M'' = \varepsilon' / \varepsilon'^2 + \varepsilon''^2 + \mathrm{i}\varepsilon'' / \varepsilon'^2 + \varepsilon''^2 \tag{5}$$

where M', M'' and ε', ε'' are the real and imaginary parts of the electric modulus and dielectric constants, respectively. The imaginary parts of the modulus at various temperatures are calculated using Eq. (5) for these ceramics. Figs. 11 and 12 show the plots of imaginary part of electric modulus (M'') with variation of frequency at few selected temperatures for CR1 and CR2. The relaxation M'' peaks are observed which shift to higher-frequency region with temperature increasing and give a direct evidence of temperature-dependent relaxation.

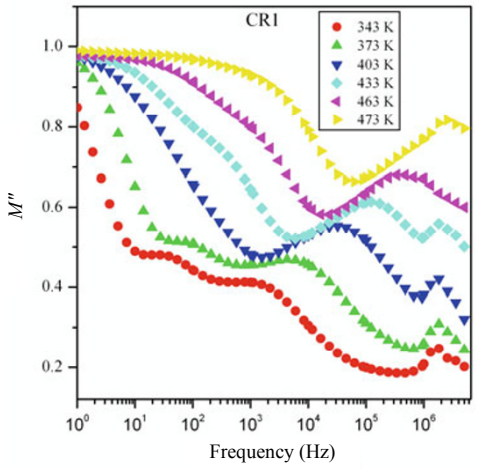

Fig. 11 Electric modulus plots of imaginary M'' vs. frequency at a few selected temperatures for CR1 sintered at 900 ℃ for 8 h.

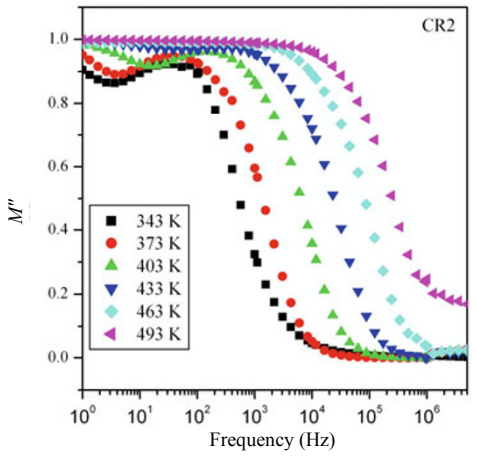

Fig. 12 Electric modulus plots of imaginary M'' vs. frequency at a few selected temperatures for CR2 sintered at 900 ℃ for 8 h.

The impedance data were also used to evaluate the relaxation time of the electrical phenomena in CR1 and CR2 ceramics using the relation $\tau = 1/\omega = 1/2\pi f$, where f is the relaxation frequency. The nature of variation of the relaxation time (τ) with reciprocal of temperature ($1/T$) is shown in Fig. 13. The activation energy in the relaxation process is determined by the temperature-dependent relaxation time constant τ_{gb} which obey Arrhenius law given by the following equation:

$$\tau = \tau_0 \exp(E_a / k_B T) \tag{6}$$

where E_a is the activation energy involved in the dielectric relaxation process; τ_0 is the pre-exponential factor; k_B is Boltzmann constant; and T is the absolute temperature. The grain boundary activation energy evaluated from the slope of $\ln\tau_{gb}$ against $1/T$ curve is found to be 0.42 eV and 0.38 eV for CR1 and CR2, respectively. This value agrees with the value reported earlier for Maxwell–Wagner relaxation arising from the interfacial polarization for CCTO ceramic which confirms the temperature dependence of dielectric properties [26,27].

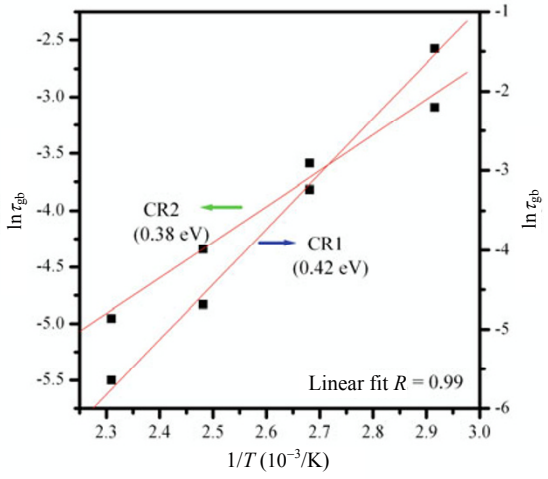

Fig. 13 Variation of relaxation time (τ_{gb}) with the inverse of temperature ($1/T$) for CR1 and CR2 ceramics.

4 Conclusions

Calcium copper titanate ceramics, $CaCu_3Ti_4O_{12}$ (CCTO), doped with La^{3+}, Mn^{2+} and Ni^{2+} at higher

concentration (5 mol% and 10 mol%) were synthesized by semi-wet route at relatively lower temperature. XRD confirms the single-phase formation of the ceramics and the scanning electron micrographs show their surface morphology with grain size in the range of 1–3 μm. The stoichiometry of the ceramics is confirmed by EDX studies. With the increase in concentration of the dopant ions in CCTO ceramics, the values of dielectric constant as well as the dielectric loss decrease. Impedance analyses of both the ceramics show that grain boundary resistance dominates the total resistance of the ceramics. The dielectric constant responses of both the ceramics arise due to the space charge polarisation. The value of resistance of the grain boundary is found to be several orders of magnitude larger than that of the grain. The nature of temperature-dependent relaxation behavior of the ceramics studied by impedance and modulus spectroscopic analyses confirms Maxwell–Wagner relaxation.

Acknowledgements

One of the authors would like to thank Prof. Om Parkash, the head of Department of Ceramic Engineering, Indian Institute of Technology, B.H.U., for extending XRD facility.

References

[1] Subramanian MA, Li D, Duan N, *et al*. High dielectric constant in $ACu_3Ti_4O_{12}$ and $ACu_3Ti_3FeO_{12}$ phases. *J Solid State Chem* 2000, **151**: 323–325.

[2] Ramirez AP, Subramanian MA, Gardel M, *et al*. Giant dielectric constant response in a copper-titanate. *Solid State Commun* 2000, **115**: 217–220.

[3] Sinclair DC, Adams TB, Morrison FD, *et al*. $CaCu_3Ti_4O_{12}$: One-step internal barrier layer capacitor. *Appl Phys Lett* 2002, **80**: 2153.

[4] Homes CC, Vogt T, Shapiro SM, *et al*. Optical response of high-dielectric-constant perovskite-related oxide. *Science* 2001, **293**: 673–676.

[5] Lunkenheimer P, Bobnar V, Pronin AV, *et al*. Origin of apparent colossal dielectric constants. *Phys Rev B* 2002, **66**: 052105.

[6] Lunkenheimer P, Fichtl R, Ebbinghaus SG, *et al*. Nonintrinsic origin of the colossal dielectric constants in $CaCu_3Ti_4O_{12}$. *Phys Rev B* 2004, **70**: 172102.

[7] Buscaglia MT, Viviani M, Buscaglia V, *et al*. Incorporation of Er^{3+} into $BaTiO_3$. *J Am Ceram Soc* 2002, **85**: 1569–1575.

[8] Bender BA, Pan MJ. The effect of processing on the giant dielectric properties of $CaCu_3Ti_4O_{12}$. *Mat Sci Eng B* 2005, **117**: 339–347.

[9] Smith AE, Calvarese TG, Sleight AW, *et al*. An anion substitution route to low loss colossal dielectric $CaCu_3Ti_4O_{12}$. *J Solid State Chem* 2009, **182**: 409–411.

[10] Singh L, Rai US, Mandal KD. Preparation and characterization of nanostructured $CaCu_{2.90}Zn_{0.10}Ti_4O_{12}$ ceramic. *Nanomater Nanotechnol* 2011, **1**: 59–66.

[11] Leret P, Fernandez J, de Frutos J, *et al*. Nonlinear *I–V* electrical behaviour of doped $CaCu_3Ti_4O_{12}$ ceramics. *J Eur Ceram Soc* 2007, **27**: 3901–3905.

[12] Mandal KD, Rai AK, Kumar D, *et al*. Dielectric properties of the $Ca_{1-x}La_xCu_3Ti_{4-x}Co_xO_{12}$ system ($x = 0.10$, 0.20 and 0.30) synthesized by semi-wet route. *J Alloys Compd* 2009, **478**: 771–776.

[13] Li M, Feteira A, Sinclair DC, *et al*. Influence of Mn doping on the semiconducting properties of $CaCu_3Ti_4O_{12}$ ceramics. *Appl Phys Lett* 2006, **88**: 232903.

[14] Rai AK, Mandal KD, Kumar D, *et al*. Dielectric properties of lanthanum-doped $CaCu_3Ti_4O_{12}$ synthesized by semi-wet route. *J Phys Chem Solids* 2009, **70**: 834–839.

[15] Shannon RD, Prewitt CT. Revised values of effective ionic radii. *Acta Cryst* 1970, **B26**: 1046–1048.

[16] Kim DW, Kim TG, Hong KS, *et al*. Low-firing of CuO-doped anatase. *Mater Res Bull* 1999, **34**: 771–781.

[17] Huang CL, Chen YC. Low temperature sintering and microwave dielectric properties of $SmAlO_3$ ceramics. *Mater Res Bull* 2002, **37**: 563–574.

[18] Ni L, Chen XM, Liu XQ. Structure and modified giant dielectric response in $CaCu_3(Ti_{1-x}Sn_x)_4O_{12}$ ceramics. *Mater Chem Phys* 2010, **124**: 982–986.

[19] Jha P, Arora P, Ganguli AK. Polymeric citrate precursor route to the synthesis of the high dielectric constant oxide, $CaCu_3Ti_4O_{12}$. *Mater Lett* 2003, **57**: 2443–2446.

[20] Singh L, Rai US, Mandal KD. Influence of Zn

doping on microstructures and dielectric properties in $CaCu_3Ti_4O_{12}$ ceramic synthesised by semiwet route. *Adv Appl Ceram* 2012, **111**: 374–380.

[21] Shao SF, Zhang JL, Zheng P, *et al*. Microstructure and electrical properties of $CaCu_3Ti_4O_{12}$ ceramics. *J Appl Phys* 2006, **99**: 084106.

[22] Yu HT, Liu HX, Hao H, *et al*. Grain size dependence of relaxor behavior in $CaCu_3Ti_4O_{12}$. *Appl Phys Lett* 2007, **91**: 222911.

[23] Hodge IM, Ingram MD, West AR. Impedance and modulus spectroscopy of polycrystalline solid electrolytes. *J Electroanal Chem Interfacial Electroch* 1976, **74**: 125–143.

[24] Fang TT, Lin WJ, Lin CY. Evidence of the ultrahigh dielectric constant of $CaSiO_3$-doped $CaCu_3Ti_4O_{12}$ from its dielectric response, impedance spectroscopy, and microstructure. *Phys Rev B* 2007, **76**: 045115.

[25] Mazni M, Daud WM, Talib SA, *et al*. AC conductivity of $Ca_{1-x}A_xCu_3Ti_4O_{12}$ (A = Sr or Ba) with $x = 0.0$ and 0.2 ceramics. *Solid State Sci Tech* 2009, **17**: 222–228.

[26] Chanmal CV, Jog JP. Dielectric relaxations in PVDF/BaTiO3 nanocomposites. *Express Polym Lett* 2008, **2**: 294–301.

[27] Zhang L, Shan XB, Wu PX, *et al*. Dielectric characteristics of $CaCu_3Ti_4O_{12}$/P(VDF-TrFE) nanocomposites. *Appl Phys A* 2012, **107**: 597–602.